Humps/Steps Influence on Stability Characteristics of Two-Dimensional Laminar Boundary Layer

Anke Wörner,* Ulrich Rist,† and Siegfried Wagner‡
University of Stuttgart, 70550 Stuttgart, Germany

The influence of two-dimensional humps and steps on the stability characteristics of a two-dimensional laminar boundary layer is investigated by means of direct numerical simulations (DNS). The localized surface irregularity is hereby modeled within the Cartesian grid by assigning body forces over surfaces that need not coincide with grid lines. Compared to the use of a body-fitted coordinate system, this method saves memory and computation time. The method is validated by grid refinement tests as well as by a comparison with water channel experiments. The DNS results for the steady flow over a rectangular hump, as well as for an instability wave traveling over a hump, show good agreement with the experimental ones. Simulation results show that a localized hump destabilizes the laminar boundary layer, whereas a forward facing step stabilizes it. The destabilization is stronger when the height or the width of the localized hump are increased. A rounded shape of the hump is less destabilizing than a rectangular shape with sharp corners. The parameter that shows the strongest influence on the stability characteristics of the boundary layer is clearly the height of the localized hump.

Nomenclature

b	=	half-width of the roughness element
F	=	dimensionless frequency parameter, $F = 2\pi \tilde{f} \tilde{v} / \tilde{U}_\infty^2 \cdot 10^6$
$\boldsymbol{F}$	=	external force field
$\boldsymbol{f}$	=	surface body force
$\tilde{f}$	=	frequency
h	=	height of the roughness element
$\tilde{L}$	=	reference length
Re	=	Reynolds number, $\tilde{U}_\infty \tilde{L} / \tilde{v}$
Re_H	=	Reynolds number based on the height of the roughness
Re_{δ_1}	=	Reynolds number based on the boundary-layer displacement thickness
t	=	time
$\tilde{U}_\infty$	=	freestream velocity
u	=	streamwise velocity component
v	=	wall-normal velocity component
x	=	streamwise coordinate
$\boldsymbol{x}_S$	=	surface of the roughness element
y	=	wall-normal coordinate
α	=	streamwise wave number
α_S	=	negative constant of the feedback algorithm
β_S	=	negative constant of the feedback algorithm
Δx	=	streamwise grid spacing
Δy	=	wall-normal grid spacing
λ_{TS}	=	Tollmien–Schlichting wavelength
$\tilde{v}$	=	kinematic viscosity
σ_x	=	half-width of the Gaussian function in x direction
σ_y	=	half-width of the Gaussian function in y direction
ω_z	=	spanwise vorticity

Superscripts

~	=	dimensional variable
'	=	disturbance variable

I. Introduction

THE specific fuel consumption of any aircraft is directly related to its drag. A major portion of aircraft drag is due to friction that is confined to the wall boundary layer of the flow. Because a turbulent boundary layer produces higher skin friction than a laminar one, the overall skin friction is highly influenced by the location of laminar–turbulent transition. By means of control, that is, delay, of laminar–turbulent transition, a reduction of the wall friction is possible. A better understanding of the mechanisms of laminar–turbulent transition is the key to being able to delay, actively or passively, transition on an airfoil.

The process of laminar–turbulent transition can be subdivided into four main stages. The first stage, the so-called receptivity, is the penetration of external perturbations into the boundary layer where they are tuned to boundary-layer disturbances. The second stage is the linear amplification of these initially created disturbances. The third one is the nonlinear development, and the last one is the breakdown to turbulence. Within this paper, we focus on the influence of surface discontinuities on the stability characteristics of a two-dimensional boundary layer within the linear range of instability.

In the manufacturing process of an airfoil, surface discontinuities such as steps at junctions or small humps are unavoidable. These surface discontinuities can influence the location of transition on the airfoil via two dominating mechanisms.

First, they are possible sources of receptivity, which means that they provide the small length scale that is necessary for the conversion process of large-scale external perturbations into small-scale boundary-layer disturbances (Ref. 1, 2, or 3). A second aspect, however, is that they are also able to either stabilize or destabilize the boundary layer locally.

The study presented here shall provide insight into the influence of surface irregularities on the amplification of Tollmien–Schlichting (TS) waves in a two-dimensional laminar boundary layer. This subject is studied by means of direct numerical simulations (DNS). A similar study was carried out by Gaster and Wang (Gaster, M., and Wang, X., "The Influence of Surface Steps on the Value of 'N' Factors Used in Estimating the Position of Transition on Aerofoils," Presented at EUROMECH Colloquium 423, Boundary-Layer Transition in Aerodynamics, April 2001). They experimentally investigated the influence of surface steps on the value of N factors used in estimating the position of transition on airfoils. They found an empirical correlation of experimental measurements of transition on a flat plate containing various steps. Within their study, it was not possible to distinguish the newly created disturbances by means of receptivity at the step from the change in stability of the boundary layer created by the presence of the step. This is only possible

by using numerical simulations where one aspect can be artificially isolated.

II.   Numerical Method

The DNS code used for the present investigation is based on a code first developed by Fasel[4] and further improved by Rist et al.,[5,6] which is used for the investigation of transition phenomena in a flat-plate boundary layer.

A.   Governing Equations

The DNS are based on the vorticity–velocity formulation of the complete Navier–Stokes equations for incompressible fluids. All spatial scales are nondimensionalized using $\tilde{L}$ and all velocities using $\tilde{U}_\infty$, where the tilde denotes dimensional variables:

$$x = \tilde{x}/\tilde{L}, \qquad u = \tilde{u}/\tilde{U}_\infty, \qquad y = \tilde{y}/\tilde{L}$$
$$v = \tilde{v}/\tilde{U}_\infty, \qquad t = \tilde{t}(\tilde{U}_\infty/\tilde{L}), \qquad Re = \tilde{U}_\infty \tilde{L}/\tilde{\nu} \qquad (1)$$

Here x denotes the wall-parallel and y the wall-normal direction; u is the velocity parallel to the flat plate.

The first step in the numerical calculation is the solution of the vorticity transport equation, which can be written as

$$\frac{\partial \omega_z}{\partial t} + \frac{\partial}{\partial x}(u \cdot \omega_z) + \frac{\partial}{\partial y}(v \cdot \omega_z) = \frac{1}{Re}\left(\frac{\partial^2 \omega_z}{\partial x^2} + \frac{\partial^2 \omega_z}{\partial y^2}\right) \qquad (2)$$

where ω_z is defined as

$$\omega_z = \frac{\partial u}{\partial y} - \frac{\partial v}{\partial x} \qquad (3)$$

Then, v can be calculated by solving the following Poisson equation:

$$\frac{\partial^2 v}{\partial x^2} + \frac{\partial^2 v}{\partial y^2} = -\frac{\partial \omega_z}{\partial x} \qquad (4)$$

The continuity equation

$$\frac{\partial u}{\partial x} + \frac{\partial v}{\partial y} = 0 \qquad (5)$$

is then used to calculate the wall-parallel velocity u.

B.   Discretization and Boundary Conditions

The flowfield is discretized using fourth-order-accurate finite differences in the streamwise (x-) and wall-normal (y-) directions on a Cartesian grid. Figure 1 shows the integration domain. The time integration is done using a fourth-order, four-step Runge–Kutta scheme. The v–Poisson equation is solved with a multigrid method, using a vectorizable, stripe-pattern successive overrelaxation (SOR) line-iteration technique on each grid. Details concerning the numerical method can be found in Ref. 5.

At the freestream boundary, the vorticity is set to zero because this boundary lies in the region of potential flow. For the wall-normal velocity v exponential decay is assumed:

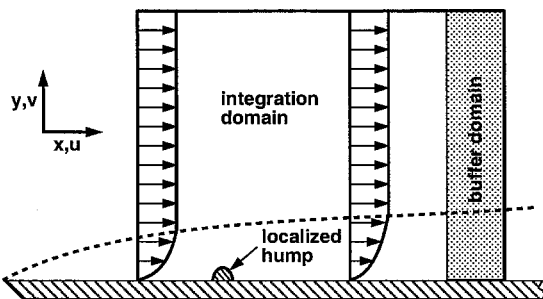$$\frac{\partial v}{\partial y} = -\alpha \cdot v \qquad (6)$$

Fig. 1   Integration domain.

Here, α is considered to be representative for the whole integration domain. In the potential flow, this condition derives the exact solution for linear TS waves with α.

At the inflow boundary, steady Falkner–Skan profiles, usually Blasius profiles, are prescribed.

Disturbances are forced by wall-normal periodic suction and blowing in a disturbance strip at the wall. Except in the disturbance strip, the no-slip and no-through-flow condition is applied at the wall.

Upstream of the outflow boundary, the unsteady vorticity is smoothly damped to the steady-state value in a buffer domain.[6] Consequently, the unsteady velocity components also decay exponentially in the streamwise direction and vanish at the outflow.

C.   Modeling of the Surface Irregularity

The localized surface irregularity within the Cartesian grid is modeled using a technique that is related to Peskin's immersed boundary approach,[7] and that has already successfully been applied, for example, by Goldstein et al.,[8] Linnick,[9] or von Terzi et al.[10] In this approach, the effect of the surface irregularity on the surrounding flowfield is modeled with an external force field that enforces no-slip and no-through-flow at selected grid points or at selected points between the grid points at every time step.

The vorticity transport equation for the two-dimensional case with an external force field $\boldsymbol{F} = (F_x, F_y)$ can be written as

$$\frac{\partial \omega_z}{\partial t} + \frac{\partial}{\partial x}(u \cdot \omega_z) + \frac{\partial}{\partial y}(v \cdot \omega_z) = \frac{1}{Re}\left(\frac{\partial^2 \omega_z}{\partial x^2} + \frac{\partial^2 \omega_z}{\partial y^2}\right)$$
$$+ \frac{\partial F_x}{\partial y} - \frac{\partial F_y}{\partial x} \qquad (7)$$

The force term on the right-hand side is the force exerted by the surface irregularity on the fluid and can be written as

$$\boldsymbol{F} = \oint \boldsymbol{f}(\boldsymbol{x}_S, t) \cdot \delta(\boldsymbol{x} - \boldsymbol{x}_S)\, \mathrm{d}S \qquad (8)$$

For numerical reasons, the delta function is approximated by a Gaussian function as follows:

$$\delta \approx \exp\left\{-[(x - x_S)/\sigma_x]^2 - [(y - y_s)/\sigma_y]^2\right\} \qquad (9)$$

The surface body force $\boldsymbol{f}$ is determined from the relation

$$\boldsymbol{f}(\boldsymbol{x}_S, t) = \alpha_S \cdot \int_0^t \boldsymbol{v}(\boldsymbol{x}_S, t')\, \mathrm{d}t' + \beta_S \cdot \boldsymbol{v}(\boldsymbol{x}_S, t) \qquad (10)$$

for surface points $\boldsymbol{x}_S$. Equation (10) represents a feedback scheme in which the velocity is used to approach the desired value iteratively.

If the surface of the irregularity is located between the grid points, the velocity at this location is interpolated from the values at the neighboring grid points using a fourth-order Lagrangian interpolation procedure.

III.   Verification and Validation

To verify the numerical scheme used, we first performed grid refinement studies in the streamwise, as well as in the wall-normal, direction. Additionally, the DNS results were compared with experimental results obtained by M. Lang in the laminar water channel of our institute. The purpose of this comparison was the validation of the method of modeling a solid surface within a Cartesian grid for the cases studied in the present paper.

A.   Grid Refinement Tests

Results of the grid refinement tests are shown in Figs. 2 and 3. Here, amplification curves for a two-dimensional TS wave with a nondimensional frequency $F = 2\pi f \nu/U_\infty^2 \cdot 10^6 = 49.34$ traveling across a rectangular hump located at $x = 4.0$ are shown. This means that the maximum of the amplitude of the streamwise disturbance velocity u' vs y is plotted against the streamwise coordinate x. The height of the hump normalized with the local boundary-layer displacement thickness δ_1 was 0.47, its half-width b was 0.1. In Fig. 2,
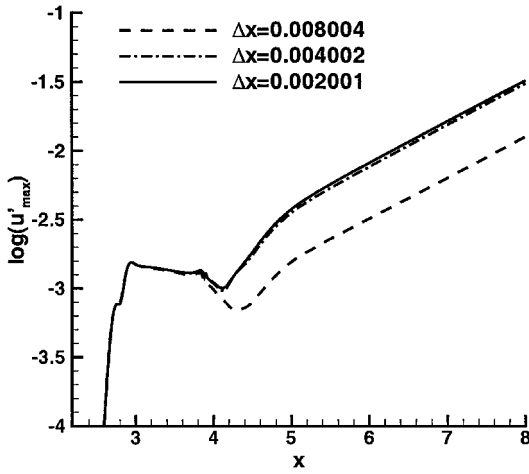
Fig. 2   Grid refinement tests in x direction; TS wave with non-dimensional frequency $F = 49.34$ traveling across a rectangular hump located at $x = 4.0$ with $h/\delta_1 = 0.47$ and $b = 0.1$.

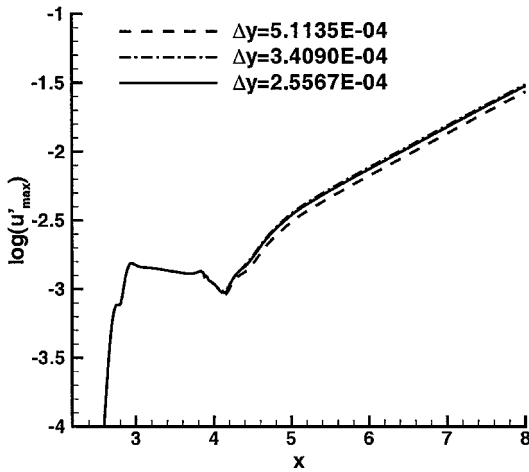
Fig. 3   Grid refinement tests in y direction; TS wave with non-dimensional frequency $F = 49.34$ traveling across a rectangular hump located at $x = 4.0$ with $h/\delta_1 = 0.47$ and $b = 0.1$.

the streamwise grid spacing is varied, whereas in Fig. 3, the wall-normal grid spacing is changed.

From Figs. 2 and 3, it is clear that the solution converges and that a resolution of 100 grid points in streamwise direction per TS wavelength ($\Delta x = 0.004002$) and 15 grid points in the wall-normal direction over the height of the hump ($\Delta y = 3.409E-04$) is a sufficient resolution for this problem.

B.   Comparison with Experiments

Figures 4–6 show a comparison of the DNS with the water channel experiment of the steady flow over a two-dimensional rectangular hump. The center of the hump is located at $x = 3.87$ ($Re_{\delta_1} = 1070$). Its height is 3 mm, its width 155 mm, giving $h/\delta_1 = 0.37$ ($Re_H = U_\infty h/\nu = 387$) and $b/\delta_1 = 19.1$. Plotted is the streamwise velocity u vs y for three different streamwise positions, one at 105 mm upstream of the center of the hump, one above the hump (at 20 mm upstream of the center), and one at 120 mm downstream of the center of the hump, approximately at the location where reattachment takes place.

The agreement found between the DNS and the experiment is quite good, which proves that the effect of the rectangular hump on the surrounding flowfield was correctly modeled by the numerical approach using an external force field.

To investigate whether unsteady effects are also correctly modeled, a second experiment was conducted in the water channel. A TS wave with a nondimensional frequency of $F = 2\pi f \nu/U_\infty^2 \cdot 10^6 = 49.34$ and an amplitude of 1% of the freestream velocity $\tilde{U}_\infty$ was created upstream of the hump, using a vibrating ribbon. This
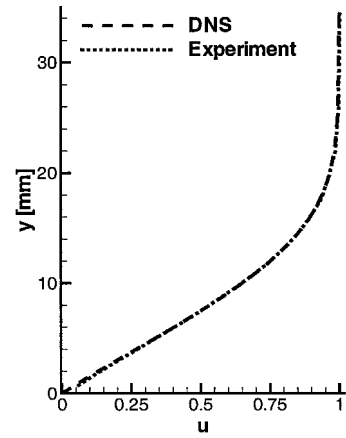

Fig. 4   Base flow upstream of the hump at $x = 3.67$ ($Re_{\delta_1} = 1042$); comparison of DNS and experiment.
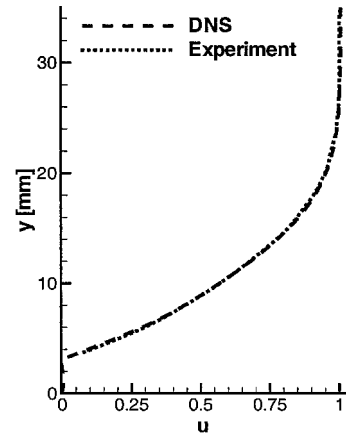

Fig. 5   Base flow above the hump at $x = 3.838$ ($Re_{\delta_1} = 1066$); comparison of DNS and experiment.
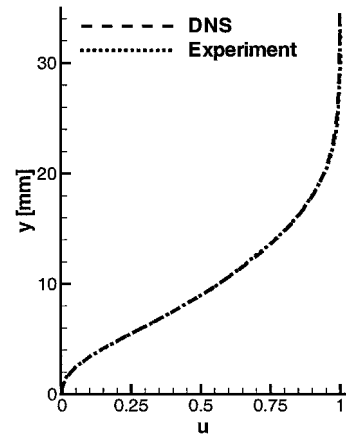

Fig. 6   Base flow downstream of the hump at $x = 4.025$ ($Re_{\delta_1} = 1091$); comparison of DNS and experiment.

TS wave has a wavelength of 310 mm, which shows that the width of the hump was chosen to be one-half of the TS wavelength. Two different cases were studied. First, the TS wave traveled along a smooth plate, whereas in a second experiment the TS wave traveled across the rectangular hump of height $h/\delta_1 = 0.37$, located at $Re_{\delta_1} = 1070$. For both experiments, the amplitude profiles of the TS wave vs y at 535 mm downstream of the center of the hump were measured.

Figure 7 compares these amplitude profiles with DNS calculations for the same two cases. In the DNS, the increase in amplitude, which is caused by the presence of the hump, is approximately 7% higher than in the experiment. This discrepancy can to some extent result
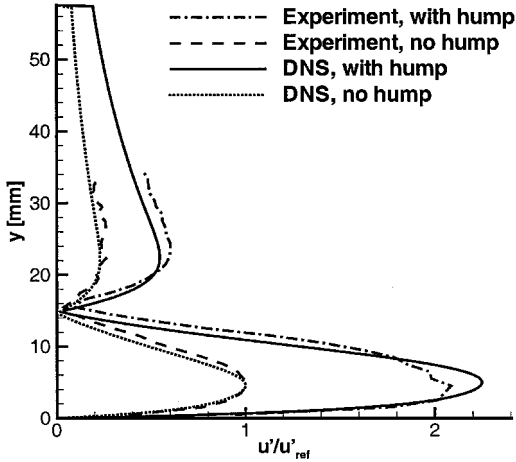
Fig. 7   Amplitude change of a TS wave traveling across a rectangular hump located at $x = 3.87$ ($Re_{\delta_1} = 1070$); profiles shown at $x = 4.56$ ($Re_{\delta_1} = 1162$); comparison of DNS and experiment.
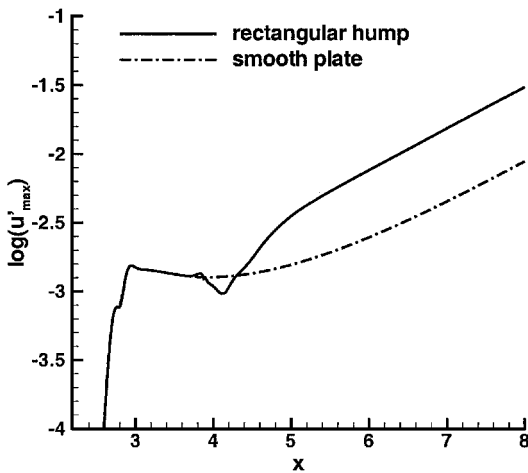

Fig. 8   Amplitude development of a TS wave with nondimensional frequency $F = 49.34$ traveling across a rectangular hump located at $x = 4.0$ with $h/\delta_1 = 0.47$ and $b = 0.1$ in comparison to a TS wave traveling along a smooth plate.

from only a few periods being time-averaged in the experiments and from there already being remarkable three-dimensional disturbances visible in the experiment at this location.

IV.   Results and Discussion

A.   Localized Hump

Figure 8 compares the amplification curve for a TS wave with a nondimensional frequency $F = 49.34$ traveling across a rectangular hump located at $x = 4.0$ ($Re_{\delta_1} = 1.72 \cdot \sqrt{(Re \cdot x)} = 1088, Re = 10^5$) to a TS wave traveling along a flat plate without any surface irregularities. The height of the hump was $h/\delta_1 = 0.47$, which corresponds to $Re_H = U_\infty h/\nu = 511$. Its width was about one-half of the wavelength of the TS wave ($b = 0.1$). The disturbance strip for the creation of the TS wave was located at $x = 2.78$ ($Re_{\delta_1} = 907$).

The influence of the hump on the TS wave traveling across it can be subdivided into two local effects that finally add up to the global effect of the hump on the TS wave far downstream of the localized hump. The local effects can be described as follows: First, at the rising edge of the hump, the amplitude of the TS wave decreases because of the thinner boundary layer that develops at the beginning of the hump. Second, at the falling edge of the hump, the amplification of the TS wave is remarkably increased compared to the wave traveling along a smooth plate. This second effect probably results from a small separation zone that forms behind the rectangular hump. Because the increase in amplification at the falling edge is stronger than the stabilizing effect that occurs at the rising edge, the global effect of a localized hump is a destabilization of the boundary layer. In the case shown in Fig. 8, the resulting amplitude of the TS

wave far downstream of the hump is about a factor of 3.2 higher than the amplitude of the TS wave traveling along a smooth plate.

Several parameters of the rectangular hump are now varied to show their influence on the amplitude development of the TS wave that travels across the hump.

1.   Influence of Height

First, the varying parameter was the height of the rectangular hump, which was changed between $h/\delta_1 = 0.235$ ($Re_H = 256$) and $h/\delta_1 = 0.94$ ($Re_H = 1023$). All other parameters were kept constant. The results of this variation are illustrated in Fig. 9. As expected, the highest hump has the largest influence on the TS wave, traveling across it. The amplitude of the TS wave far downstream of the hump increases by a factor of 1.4 for $Re_H = 256$, 3.2 for $Re_H = 511$, and 26.0 for $Re_H = 1023$ by the presence of the hump. This shows that up to a height of $Re_H = 511$ the increase in amplitude of the TS wave scales approximately linear with the height of the rectangular hump. For $Re_H = 1023$, this dependence becomes nonlinear because the stability characteristics of the boundary layer are dramatically changed. Another hint for this large change in the stability characteristics is the completely different slope of the amplification curve downstream of the hump, compared to the cases with smaller humps.

2.   Influence of Width

Then, the width of the rectangular hump is changed. The results of this variation can be found in Fig. 10. The width was varied between $b = 0.1$ and 0.4, the wavelength of the TS wave is approximately $\lambda_{TS} = 0.2$. The height was $h/\delta_1 = 0.47$ ($Re_H = 511$). The largest influence on the TS wave is observed for the hump with the largest
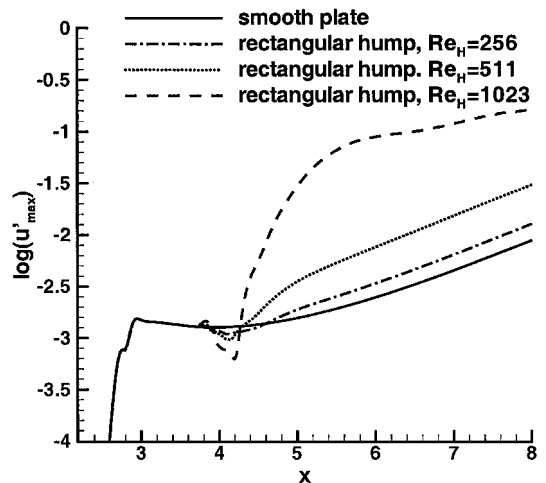

Fig. 9   Amplitude development of a TS wave with $F = 49.34$ traveling across a hump located at $x = 4.0$ with varying height and $b = 0.1$.
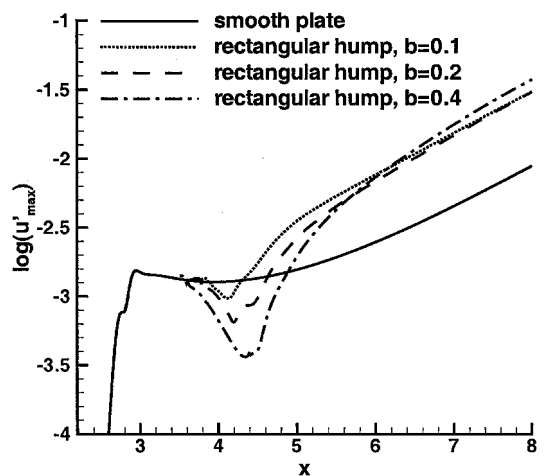

Fig. 10   Amplitude development of a TS wave with $F = 49.34$ traveling across a hump located at $x = 4.0$ with $h/\delta_1 = 0.47$ and varying width.
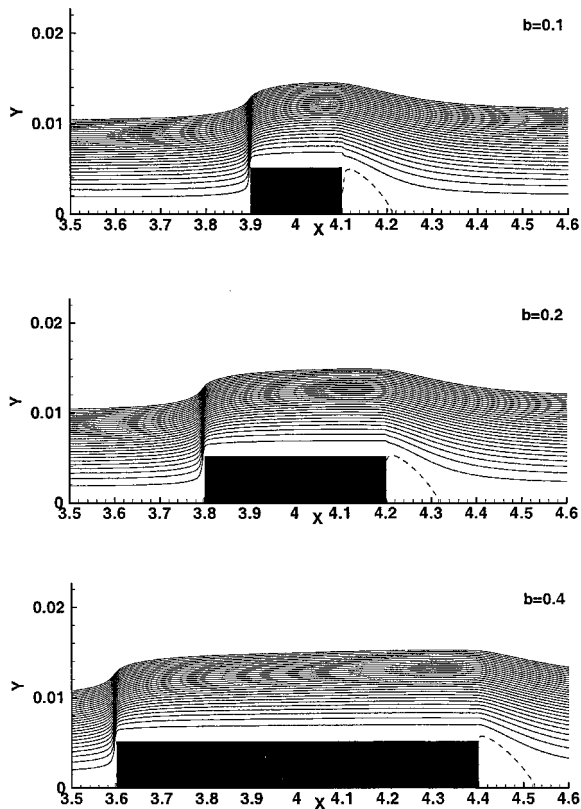
Fig. 11   Streamlines in the vicinity of the localized hump for humps located at $x = 4.0$ with width: a) $b = 0.1$, b) $b = 0.2$, and c) $b = 0.4$ and a constant height of $h/\delta_1 = 0.47$; - - - -, separation streamline.

width. Nevertheless, the parameter that has the most influence on the amplitude increase of the TS wave is clearly the height of the hump. The width of the hump plays only a minor role.

An insight into the flowfield for the three different cases with humps of different widths is given in Fig. 11, where streamlines in the vicinity of the hump are plotted. The separation streamline is marked by a dashed line. The y direction in this plot is stretched by a factor of 20. For the case with the smallest width, the resolution in the x direction for the calculation of the streamlines had to be twice as high ($\Delta x = 0.002001$) compared to the other two cases ($\Delta x = 0.004002$). This increase in resolution was only necessary for the calculation of the streamlines. As can be seen in Fig. 2, the higher resolution has no effect on the influence of the hump on the TS wave. Figure 11 shows that the separation zone behind the hump increases with increasing width of the hump. This leads to the following behavior: As the hump gets wider, the length of the zone in which the TS wave attenuates gets longer. At the same time, the amplification zone behind the hump gets larger and stronger. Because those two effects almost cancel each other, the width of the hump has almost no influence on the resulting amplitude of the TS wave far downstream.

3. Influence of Shape

In Fig. 12, the amplitude development of three TS waves can be observed. One travels over a rectangular hump, one over a rounded hump, the shape of which is a quadratic function of x, and one travels over a smooth plate. The height of both humps is $h/\delta_1 = 0.47$ ($Re_H = 511$), the width is $b = 0.1$. The rectangular hump with its sharp corners has, as could be expected, the most influence on the stability characteristic of the boundary layer.

B.   Forward-Facing Step

Figure 13 shows the amplification curve for a TS wave traveling across a forward-facing step compared to a TS wave traveling along a perfectly smooth flat plate. The nondimensional frequency is the same as before. The forward-facing step is located at $x = 4.0$, which corresponds to $Re_{\delta_1} = 1088$. Its height normalized with δ_1 is 0.235 ($Re_H = 256$).
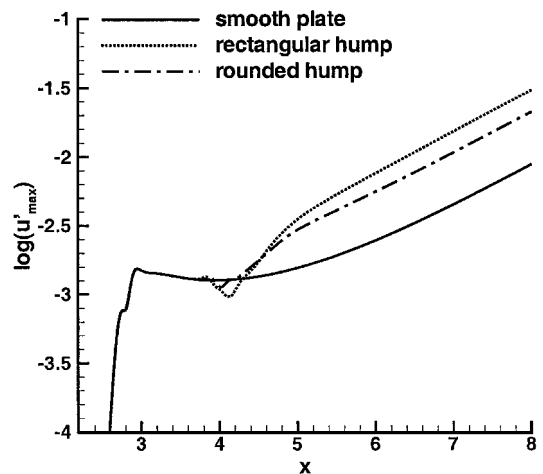

Fig. 12   Amplitude development of a TS wave with $F = 49.34$ traveling across a hump of different shape located at $x = 4.0$ with $h/\delta_1 = 0.47$ and $b = 0.1$.
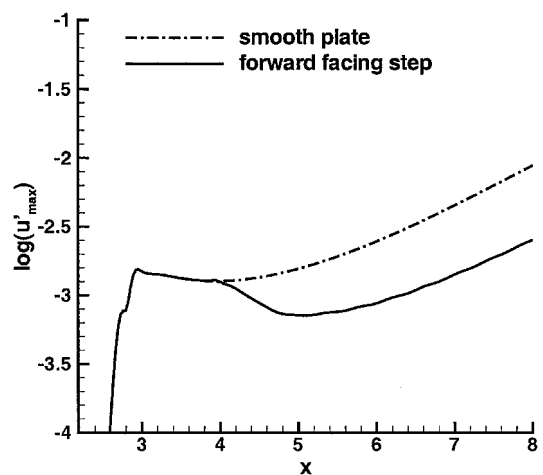

Fig. 13   Amplitude development of a TS wave with $F = 49.34$ traveling across a forward-facing step located at $x = 4.0$ with $h/\delta_1 = 0.235$.

As can be seen, the amplitude of the TS wave is now reduced by the forward-facing step because the thinner boundary layer evolving on the step is more stable than the boundary layer on the smooth plate. The separation zone in front of the step is very small and, therefore, has no influence on the TS wave. This reduction in amplitude seems surprising, but results from the freestream disturbances being absent in the simulation. This means that no receptivity can take place, which, in reality, would add additional disturbances.

V.   Conclusions

By means of DNS, the influence of humps and steps on the stability characteristics of a two-dimensional laminar boundary layer has been investigated. The localized surface irregularity was modeled within a Cartesian grid using an immersed boundary technique, where the influence of a solid wall on the surrounding flowfield is modeled by using an external force field that enforces no-slip and no-through-flow conditions on the solid wall. This approach was validated by comparing the DNS results with measurements conducted in the laminar water tunnel of our institute. For a steady as well as an unsteady test case, the DNS results were in good agreement with the experimental results. This showed that the effect of a localized hump on the surrounding flowfield was correctly modeled by the immersed boundary technique.

A localized hump was found to have an overall destabilizing effect on the laminar boundary layer, whereas a forward-facing step showed a stabilizing effect. The destabilization of the boundary layer by the presence of a hump results from the combination of two local phenomena. The TS wave is first damped by the stabilizing effect of the rising edge of the hump, with its thinner boundary layer, as

can also be seen for the forward-facing step. At the falling edge of the hump, the amplification is locally highly increased by the presence of a small separation zone behind the hump. This increase in amplification is much stronger than the damping caused by the rising edge of the hump. Therefore, the overall effect of a localized hump is a destabilization of the boundary layer. For the localized hump, the influence of several parameters on the destabilization was investigated. Up to a height, normalized with the local displacement thickness, of approximately $h/\delta_1 = 0.5$, the increase in amplitude of a TS wave traveling across the hump was found to depend linearly on the height of the hump. For a height of $h/\delta_1 = 0.97$, this dependence was clearly nonlinear. If the width of the hump was increased, the effect on the TS wave was also found to be larger, but the influence of the width was weaker than the influence of the height of the hump. Additionally, the shape of the hump was varied. A rectangular hump with sharp corners showed a larger influence on the amplitude development of a TS wave than a rounded hump, the shape of which was a quadratic function of x.

In the future, the immersed boundary technique is planned for use for numerical simulations of roughness acoustic receptivity. Additionally, the approach will be extended to be able to deal with three-dimensional surface irregularities.

Acknowledgments

References

[1]Choudhari, M., and Streett, C. L., "A Finite Reynolds-Number Approach for the Prediction of Boundary-Layer Receptivity in Localized Regions," *Physics of Fluids, A*, Vol. 4, No. 11, 1992, pp. 2495–2514.

[2]Crouch, J. D., "Localized Receptivity of Boundary Layers," *Physics of Fluids A*, Vol. 4, No. 7, 1992, pp. 1408–1414.

[3]Goldstein, M. E., "Scattering of Acoustic Waves into Tollmien–Schlichting Waves by Small Streamwise Variations in Surface Geometry," *Journal of Fluid Mechanics*, Vol. 154, 1985, pp. 509–529.

[4]Fasel, H. F., "Investigation of the Stability of Boundary Layers by a Finite-Difference Model of the Navier–Stokes Equations," *Journal of Fluid Mechanics*, Vol. 18, 1976, pp. 355–383.

[5]Rist, U., and Fasel, H., "Direct Numerical Simulation of Controlled Transition in a Flat-Plate Boundary Layer," *Journal of Fluid Mechanics*, Vol. 298, 1995, pp. 211–248.

[6]Kloker, M., Konzelmann, U., and Fasel, H., "Outflow Boundary Conditions for Spatial Navier–Stokes Simulations of Transitional Boundary Layers," *AIAA Journal*, Vol. 31, No. 4, 1993, pp. 620–628.

[7]Peskin, C. S., "Numerical Analysis of Blood Flow in the Heart," *Journal of Computational Physics*, Vol. 25, No. 3, 1977, pp. 220–252.

[8]Goldstein, D., Handler, R., and Sirovich, L., "Modeling a No-Slip Flow Boundary with an External Force Field," *Journal of Computational Physics*, Vol. 105, No. 2, 1993, pp. 354–366.

[9]Linnick, M. N., "Investigation of Actuators for Use in Active Flow Control," M.S. Thesis, Dept. of Aerospace and Mechanical Engineering, Univ. of Arizona, Tucson, AZ, 1999.

[10]von Terzi, D. A., Linnick, M. N., Seidel, J., and Fasel, H., "Immersed Boundary Techniques for High-Order Finite-Difference Methods," AIAA Paper 2001-2918, June 2001.

P. Givi
Associate Editor